Korean J. Chem. Eng., **19**(3), 391-399 (2002)

Mathematical Modeling for Chemical Vapor Deposition in a Single-Wafer Reactor: Application to Low-Pressure Deposition of Tungsten

Jung-Hwan Park†

Dept. of Chemical and Environmental Technology, Inha Technical College, Incheon 402-752, Korea
(*Received 8 March 2001 • accepted 8 August 2001*)

Abstract–A mathematical model for low pressure chemical vapor deposition in a single-wafer reactor in stagnation point flow has been developed to investigate the reactor performance. The transient transport equations for a simulated reactor include continuity, momentum, energy, and gaseous species balances. The model equations are simultaneously solved by using a numerical technique of orthogonal collocation on finite element method. Simulation studies have been performed to gain an understanding of tungsten low pressure chemical vapor deposition process. The model is then used to optimize the deposition rate and uniformity on a wafer, and the effects of operating conditions on deposition rate are studied to examine how system responses are affected by changes in process parameters. Deposition rate and uniformity calculated at the steady state are observed to be very sensitive to both temperature and total pressure. In addition, the model predictions for tungsten deposition from hydrogen reduction of tungsten hexafluoride have been compared with available experimental data in order to demonstrate the validity of the model.

Key words: Chemical Vapor Deposition, Tungsten Deposition, Single-Wafer Reactor, Deposition Rate, Process Simulation

INTRODUCTION

Process simulation plays an important role in integrated circuit (IC) development in many ways. For example, it can assist equipment designers and process engineers to establish reliable chemical vapor deposition (CVD) and other processes in the microelectronic field [Werner et al., 1992]. As more complex and expensive equipment is adopted in the semiconductor industry, process simulation is expected to play an increasing role in the analysis and design of novel CVD systems. Although experimental validation of the predicted results is still necessary, computer simulation can reduce the required experimental time and costs. Reactor scale modeling is an excellent tool for improving our understanding of the chemical and physical phenomena involved in CVD reactors as well as for testing new reactor configurations without actually "cutting metal." New reactor designs might be inspired through simulation efforts. In addition, optimization of CVD reactors and processes could be greatly enhanced through simulation.

In the IC industry, the use of CVD processes during device fabrication is widespread for the deposition of epitaxial silicon, polysilicon, silicon dioxide, and silicon nitride films, as well as conducting materials such as tungsten and aluminum [Skelly et al., 1987]. Despite this wide range of applications in the modern IC industry, CVD reactors are perhaps the least understood dynamic units in the device manufacturing process. Although numerous modeling studies of CVD reactors have been performed [Hess et al., 1985; Jensen, 1987], this area is not as well established as the modeling of conventional chemical reactors, such as catalytic packed bed reactors. One major reason for this is that information on the kinetic parameters for CVD reactions is relatively incomplete. Improved CVD reactors are critical for present and future development of very large scale integrated (VLSI) and ultra large scale integrated (ULSI) applications. Trends toward large diameter silicon wafers, particularly when combined with decreasing dimensions in integrated circuits, make these demands become more stringent [Bullis and O'Mara, 1993; Moslehi et al., 1992].

An approach to understanding the behavior of CVD reactors is to simulate the reactor models. The main goal of reactor modeling is to relate performance measures (e.g., film deposition rate, uniformity, composition) to operating conditions (e.g., pressure, temperature, and flow rates) and reactor geometry. Besides performance predictions, mathematical modeling can provide guidance for process optimization, chemical kinetic parameter estimation, and improved reactor designs. A realistic mathematical model provides quantitative predictions of film thickness and composition uniformity. To obtain films which possess satisfactory properties, it is crucial to realize which deposition variables affect film properties and how the deposition variables affect the properties. Ideally, a model predicts process performance as functions of process parameters for different chemistries and reactor designs. Unfortunately, the relationship between process results and process variables is often complicated and is poorly understood. Therefore, it is critical to know how operating conditions impact the uniformity of deposited films across a wafer as well as in features on patterned wafers.

Single-wafer reactors (SWRs), which have flow fields that are better defined than conventional volume-loaded multiple wafer reactors (MWRs), are often preferred to MWRs, because they offer the possibility of superior deposition thickness uniformity at higher conversion levels of costly reactants. Some comparisons between SWRs and MWRs have been discussed in the literature [Lam and Koch, 1980; McConica, 1988; Cale et al., 1990; Moslehi et al., 1992]. Recently, interest in SWRs has grown considerably for chemical vapor deposition processes [Kleijn et al., 1989; Jasinski and Kang, 1991; Rode and Schmitz, 1992; Dobskin, 1992; Cale et al., 1993], for etching processes [Economou and Alkire, 1988; Park and Economou,

†To whom correspondence should be addressed.
E-mail: jhpark@true.inhatc.ac.kr

1990; Riely and Clark, 1991] and for rapid thermal processing [Wong, 1989; Campbell et al., 1990; Chatterjee et al., 1992]. Mathematical models for tungsten deposition in cold-wall SWRs have been published recently [Ulacia et al., 1989; Jasinski and Harshbarger, 1989; Hasper et al., 1990; Kleijn et al., 1991; Jasinski and Kang, 1991; Werner et al., 1992; Park, 1996a]. Some models have been based on commercially available SWRs and used simplified assumptions. In order to model blanket tungsten low pressure CVD (LPCVD) from H_2-WF_6 system in a SWR, the transient two-dimensional LPCVD model is discussed in this study. This model has been used to study startup transients [Cale et al., 1991, 1992; Park, 1996b], but the transients are not considered in this paper; i.e., the transient reactor model is used to obtain steady state solutions.

The overall objective of this paper is to demonstrate how simulations can be used to gain an understanding of LPCVD processes. This goal is achieved in the following two ways. First, a transient model describing the fluid dynamics, heat and mass transport, and chemical reactions in a stagnation point flow apparatus, incorporating all the relevant phenomena; e.g., multicomponent thermal diffusion, buoyancy-driven flow, the Dufour effect, homogeneous and heterogeneous reactions, and variable gas properties, is developed to study the effects of operating conditions and reactor geometry on the wafer film thickness and composition uniformity. This model may be applied to a large variety of CVD processes and reactors. Secondly, the predictions of deposition rates are compared with some available experimental data published in the literature for blanket tungsten deposition in order to ensure the single-wafer reactor model used to be reliable.

TUNGSTEN LPCVD CHEMISTRY

Tungsten has received widespread attention for metallization IC technology [Blewer, 1986; Broadbent, 1987; Blewer and McConica, 1989; Smith and Blumenthal, 1991; Rana et al., 1992]. Tungsten appears to be an excellent candidate material for interconnect applications because of its low resistance, low stress and conformal step coverage. Tungsten CVD is performed in either a selective or a blanket mode. The process mode is determined by the process chemistry, the reactor geometry, the process conditions and the patterned wafer surface. Blanket tungsten LPCVD by the hydrogen reduction of tungsten hexafluoride is considered in this study. The stoichiometry of blanket tungsten deposition films by the hydrogen reduction of WF_6 is

$$WF_6+3H_2 \rightarrow W+6HF. \quad (1)$$

The kinetics of this reaction have been studied by many researchers [Bryant, 1978; Broadbent and Ramiller, 1984; Pauleau and Lami, 1985; McConica and Krishnamani, 1986; van der Putte, 1987]. For sufficiently high concentration of WF_6, the reaction rate was found to depend upon the temperature and the hydrogen partial pressure. Most investigators agree that the reaction rate is half order in hydrogen and zero order in WF_6 partial pressure at high enough WF_6 partial pressures. However, at very low pressures of WF_6, a modified rate expression has been proposed to make the rate approach zero as the WF_6 partial pressure approaches zero [Cale et al., 1993; Park, 1996b]. As a result, the intrinsic surface reaction rate can be approximately represented by

$$\Re = \frac{1.0\exp[-8300/T]P_{H_2}^{0.5}P_{WF_6}}{1+450P_{WF_6}} \quad (2)$$

where p_{H2} and p_{WF6} are the local partial pressures of hydrogen and WF_6 in Torr. Eq. (2) is based on an analysis of deposition rate data in the literature [Broadbent and Ramiller, 1984; van der Putte, 1987; Kelijn et al., 1991]. It is notable that this expression can reduce to the usually reported half order dependence on hydrogen partial pressure for significant WF_6 partial pressures.

TRANSPORT EQUATIONS FOR 2-D FLOW IN A SINGLE-WAFER REACTOR

A general mathematical model of a CVD reactor consists of a set of partial differential equations, which includes the fluid dynamics as well as heat and mass transport phenomena along with boundary conditions, incorporating all the chemical and physical processes; e.g., multicomponent thermal diffusion, buoyancy driven flow, the Dufour effect, homogeneous and heterogeneous reactions, and variable gas properties. A transient CVD model for an SWR in stagnation point flow is developed. The reactor modeled is representative of commercial single-wafer reactor designs in which the source gas enters from the top and flows over the wafer mounted on the susceptor (Fig. 1), which is similar to that used in the literature [Kleijn, 1991; Cale et al., 1993; Park, 1996a]. In developing the model, the major assumptions used are:

1. Gases are ideal.
2. The gas flow is laminar and axisymmetric.
3. The fluid behaves as a continuum.
4. Radiant heat transfer is negligible.
5. Contributions of heat flux from viscous dissipation and pressure changes are ignored.
6. Gas phase reactions are ignored.
7. Contributions of mass flux from pressure diffusion and forced diffusion are neglected.
8. There is no deposition on solid surfaces other than susceptor and wafer surfaces.

1. Transport Equations

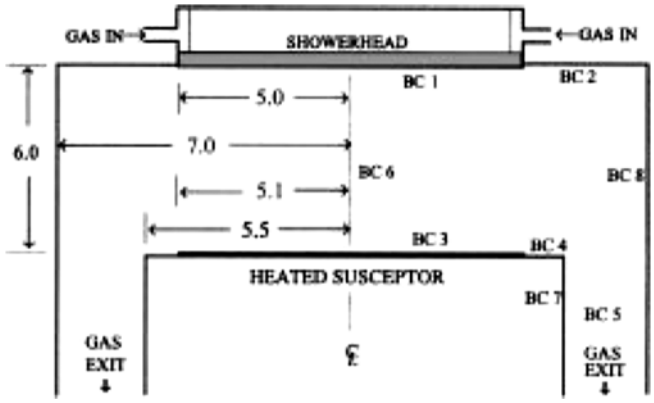

Fig. 1. Schematic diagram of single-wafer reactor chamber, along with reactor dimensions in centimeters. BC number represents the surface on which the boundary condition is applied.

Based on these assumptions, each of the conservation equations can be written explicitly in cylindrical coordinates. Since the flow is assumed to be axially symmetric for the modeled vertical CVD reactor, all of the dependent variables are independent of angular direction. The governing equations thus depend only on the coordinate z in the axial direction and on the coordinate r in the radial direction. Based on this observation, the modeling equations may be written in scalar form as follows:

Continuity equation

$$\frac{\partial \rho}{\partial t}+\frac{1}{r}\frac{\partial}{\partial r}(\rho r v_r)+\frac{\partial}{\partial z}(\rho v_z)=0 \tag{3}$$

Momentum equations

r-direction

$$\rho\left(\frac{\partial v_r}{\partial t}+v_r\frac{\partial v_r}{\partial r}+v_z\frac{\partial v_r}{\partial z}\right)=-\frac{\partial P}{\partial r}+\frac{1}{r}\frac{\partial}{\partial r}\left[\mu r\left\{\frac{4}{3}\frac{\partial v_r}{\partial r}-\frac{2}{3}\left(\frac{v_r}{r}+\frac{\partial v_z}{\partial z}\right)\right\}\right]-\frac{\mu}{r}\left\{\frac{4}{3}\frac{v_r}{r}-\frac{2}{3}\left(\frac{\partial v_r}{\partial r}+\frac{\partial v_z}{\partial z}\right)\right\}+\frac{\partial}{\partial z}\left\{\mu\left(\frac{\partial v_z}{\partial r}+\frac{\partial v_r}{\partial z}\right)\right\} \tag{4}$$

z-direction

$$\rho\left(\frac{\partial v_z}{\partial t}+v_r\frac{\partial v_z}{\partial r}+v_z\frac{\partial v_z}{\partial z}\right)=-\frac{\partial P}{\partial z}+\frac{1}{r}\frac{\partial}{\partial r}\left\{\mu r\left(\frac{\partial v_z}{\partial r}+\frac{\partial v_r}{\partial z}\right)\right\}+\frac{\partial}{\partial z}\left[\mu\left\{\frac{4}{3}\frac{\partial v_z}{\partial z}-\frac{2}{3}\left(\frac{v_r}{r}+\frac{\partial v_r}{\partial r}\right)\right\}\right]+\rho g \tag{5}$$

Energy balance equation

$$\rho c_p\left(\frac{\partial T}{\partial t}+v_r\frac{\partial T}{\partial r}+v_z\frac{\partial T}{\partial z}\right)=\frac{1}{r}\frac{\partial}{\partial r}\left(\lambda r\frac{\partial T}{\partial r}\right)+\frac{\partial}{\partial z}\left(\lambda\frac{\partial T}{\partial z}\right)+\frac{1}{r}\frac{\partial}{\partial r}\left(R_g T\sum_{i=1}^{n}\frac{D_i^T}{m_i x_i}r\frac{\partial x_i}{\partial r}\right)+\frac{\partial}{\partial z}\left(R_g T\sum_{i=1}^{n}\frac{D_i^T}{m_i x_i}\frac{\partial x_i}{\partial z}\right) \tag{6}$$

Species balance equations

$$\rho\left(\frac{\partial \omega_i}{\partial t}+v_r\frac{\partial \omega_i}{\partial r}+v_z\frac{\partial \omega_i}{\partial z}\right)=\frac{1}{r}\frac{\partial}{\partial r}\left(\rho D_{im} r\frac{\partial \omega_i}{\partial r}\right)+\frac{\partial}{\partial z}\left(\rho D_{im}\frac{\partial \omega_i}{\partial z}\right)+\frac{1}{r}\frac{\partial}{\partial r}\left(\frac{D_i^T}{T}r\frac{\partial T}{\partial r}\right)+\frac{\partial}{\partial z}\left(\frac{D_i^T}{T}\frac{\partial T}{\partial z}\right) \tag{7}$$

Variables and parameters are defined in the List of Symbols. Note that there are n−1 independent species balance equations, with the composition of the nth species determined by using the constraint that the sum of the mass fractions is one. The last two terms in the bracket of Eq. (6) represent the thermal diffusion (Soret effect), which occurs when gas molecules experience a driving force due to temperature gradients. This effect is usually insignificant compared with ordinary diffusion. However, the Soret effect can play a significant role in cold wall reactors due to both steep temperature gradients near the hot susceptor and differences in molecular weights among gaseous components. In the presence of temperature gradients, the heavier and larger molecules tend to concentrate in the colder regions, whereas the lighter and smaller molecules move towards the hotter regions. The last two terms of Eq. (7) represent the Dufour energy flux resulting from concentration gradients in each direction, which is the reciprocal process to thermal diffusion.

2. Boundary Conditions and Initial Conditions

Boundary conditions for the velocity, the temperature and the species concentrations must be specified at the reactor inlet, the outlet, and the centerline, on the reactor walls as well as on the wafer and susceptor surfaces. The boundary conditions on the SWR are the following, where the number refers to the position in the reactor as shown in Fig. 1.

BC 1: $v_r=0,\ v_z=v_0,\ T=T_0,\ \omega_i=\omega_{i,0}$ (8)

BC 2: $v_r=0,\ v_z=0,\ T=T_w,\ \rho D_{im}\frac{\partial \omega_i}{\partial z}+D_i^T\frac{\partial}{\partial z}(\ln T)=0$ (9)

BC 3: $v_r=0,\ v_z=-\frac{1}{\rho}\sum_{i=1}^{n}m_i v_i \Re,\ T=T_s,$

$$\rho D_{im}\frac{\partial \omega_i}{\partial z}+D_i^T\frac{\partial}{\partial z}(\ln T)=m_i v_i \Re \tag{10}$$

BC 4: $v_r=0,\ v_z=-\frac{1}{\rho}\sum_{i=1}^{n}m_i v_i \Re,\ \frac{\partial T}{\partial z}=0,$

$$\rho D_{im}\frac{\partial \omega_i}{\partial z}+D_i^T\frac{\partial}{\partial z}(\ln T)=m_i v_i \Re \tag{11}$$

BC 5: $v_r=0,\ \frac{\partial v_z}{\partial z}=0,\ \frac{\partial T}{\partial z}=0,\ \frac{\partial \omega_i}{\partial z}=0$ (12)

BC 6: $v_r=0,\ \frac{\partial v_z}{\partial r}=0,\ \frac{\partial T}{\partial r}=0,\ \frac{\partial \omega_i}{\partial r}=0$ (13)

BC 7: $v_r=0,\ v_z=0,\ \frac{\partial T}{\partial r}=0,\ \rho D_{im}\frac{\partial \omega_i}{\partial r}+D_i^T\frac{\partial}{\partial r}(\ln T)=0$ (14)

BC 8: $v_r=0,\ v_z=0,\ T=T_w,\ \rho D_{im}\frac{\partial \omega_i}{\partial r}+D_i^T\frac{\partial}{\partial r}(\ln T)=0$. (15)

It is noted that an uniform gas velocity is used at the reactor inlet. The use of plug flow is quite reasonable for the showerhead rather than the use of well developed flow [Fitzjohn and Holstein, 1990]. There is a finite normal velocity component at the reactive surfaces because of the surface reactions. On the reactive surfaces, the net mass flux normal to the surface equals the rate of surface reactions, as indicated in Eq. (2). The local film growth rate in Å/min, in terms of the surface reaction, is

$$G=5.72\times10^{10}\,\Re. \tag{16}$$

The total pressure is specified at the reactor outlet, where it is often measured in practice.

The appropriate initial conditions depend how the process runs. The susceptor temperature can be ramped up from a certain temperature after the reactant flow rates have been established or *vice versa*. These startup transients have been studied [Cale et al., 1991, 1992; Park, 1996b]. However, we ignore these transients and focus on steady state predictions in this paper even though the transient equations are used to solve a set of partial differential equations.

3. Estimation of Transport Coefficients

The transport coefficients for the gas mixture are functions of temperature, pressure, and composition of the gas mixture. The estimation of transport properties is based on reliable theory and empirical rules [Reid et al., 1988; Hirschfelder et al., 1954; Chase et al., 1985; Pankratz, 1984]. A detailed computation of transport coefficients is described in the appendix. For computation, local values

for transport coefficients are calculated at local temperature, pressure, and concentration in the gas phase.

4. Numerical Solution Method

Orthogonal collocation on finite elements (OCFE) with Lagrange polynomials is used to solve a set of transient partial differential equations. This approach is a method of weighted residuals and is very attractive in terms of the required computational effort and accuracy [Finlayson, 1980; Suwondo et al., 1991]. In OCFE, the solution domain is divided into many discrete rectangular subdomains that fill the entire spatial region. The axisymmetric half of the cylindrical domain has been discretized on a nonuniform grid, which consists of 31 nodes in the axial direction and 28 nodes in the radial direction. The use of OCFE removes the spatial derivatives, converting the set of nonlinear partial differential equations to a set of nonlinear ordinary differential equations (ODEs) in time. The set of nonlinear ODEs along with algebraic equations resulting from the boundary conditions can be readily solved by using an available nonlinear ODE solver, such as IMSL routines. The initial values for the dependent variables at each point are determined in advance under no reaction conditions (inert gas feeding condition) by solving the steady state momentum and energy balance equations. The reason is that deposition processes commonly used in microelectronic devices run with inert gas until establishing fully developed velocity and susceptor temperature in the reactor. More details about the solution technique are available in the literature [Park, 1992].

RESULTS AND DISCUSSION

1. Results of Steady State Simulation

The dimensions of the reactor used in the simulation are given in Fig. 1 in centimeter units. The gases are introduced at the top through a showerhead nozzle and flow towards a susceptor perpendicular to the incoming gas stream. The wafer is placed on the top of the heated susceptor. The reactor dimensions and operating conditions are chosen to be similar to those used in commercial single-wafer reactor designs. A four-inch wafer is considered in this study. Although either larger or smaller wafers are used in the semiconductor industry, the modeling strategy would be identical. The reactor wall temperature is assumed to be constant and uniform at 300 K,

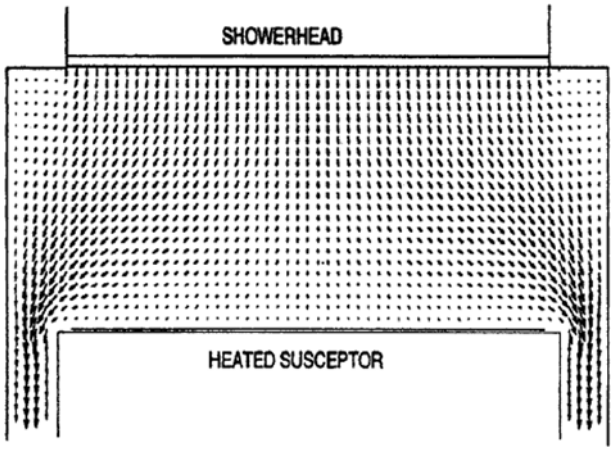

Fig. 2. Flow velocity vectors in the reactor.

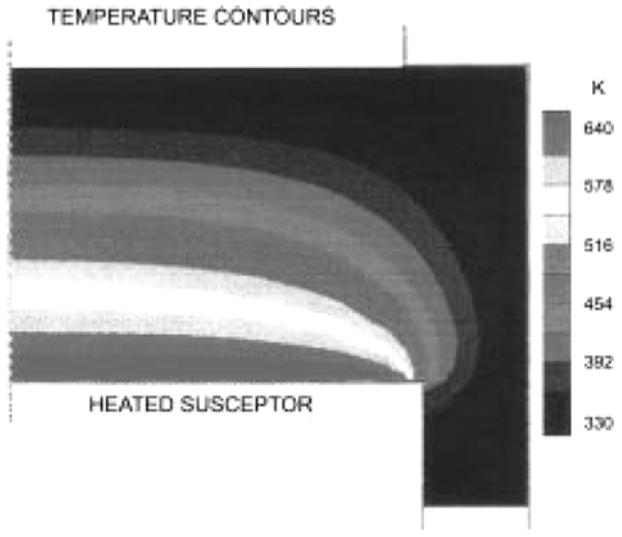

Fig. 3. Calculated isotherms in a half of the reactor.

which is also the assumed temperature of the feed gas. The wafer temperature is assumed to be the same as the heated susceptor temperature, 673 K. The operating outlet pressure is kept as 1.0 torr. The H_2 flow rate is 570 sccm, the WF_6 flow is 30 sccm, and the inert gas (argon) flow is 60 sccm.

Figs. 2-6 summarize the steady state results of the mathematical model computations. Fig. 2 shows the calculated gas flow. The length of each arrow indicates the local velocity in a relative scale, and it points in the direction of the local mass velocity. The axial velocity component has its same value at the reactor inlet due to the use of plug flow, which is assumed in the showerhead. The use of the showerhead can suppress the recirculation of gases in the SWR [Fitzjohn and Hlostein, 1990]. Beyond the susceptor edge the velocity profile is nearly parabolic with a zero radial component. At higher pressures and smaller flow rates, significant buoyancy-driven recirculation might occur in the flow. Fig. 3 shows the isotherms in a half of the reactor. The temperature increases as the gas approaches the hot susceptor and a large local temperature gradient is observed. The Dufour effect has been proved not to impact the calculated temperatures for the operating conditions used in this study. This observation is consistent with previous simulation results in LPCVD processes [Jenkinson and Pollard, 1984; Kleijn et al., 1991; Kleijn, 1991].

The primary motivation for calculating the species concentration distributions in the reactor is to predict the local film deposition rate and resulting film uniformity on the substrate surface as well as to predict the step coverage (conformality) in and over features on patterned wafers. Species concentration calculated by the reactor model has been used to estimate the step coverage in a rectangular trench for the feature scale model [Cale et al., 1992, 1993; Park, 1996a, b]. Figs. 4a-4b illustrate contours of mole fractions for WF_6 and H_2, respectively. The concentration of reactive gases decreases towards the susceptor due to the tungsten deposition at the wafer. It can be seen that the mole fractions of the reactants decrease as the wafer surface is approached due to consumption of the reactant gases resulting from surface reactions. Significant radial concentration gradients exist along the wafer, becoming more pronounced towards the wafer edge. Hydrogen concentrates some-

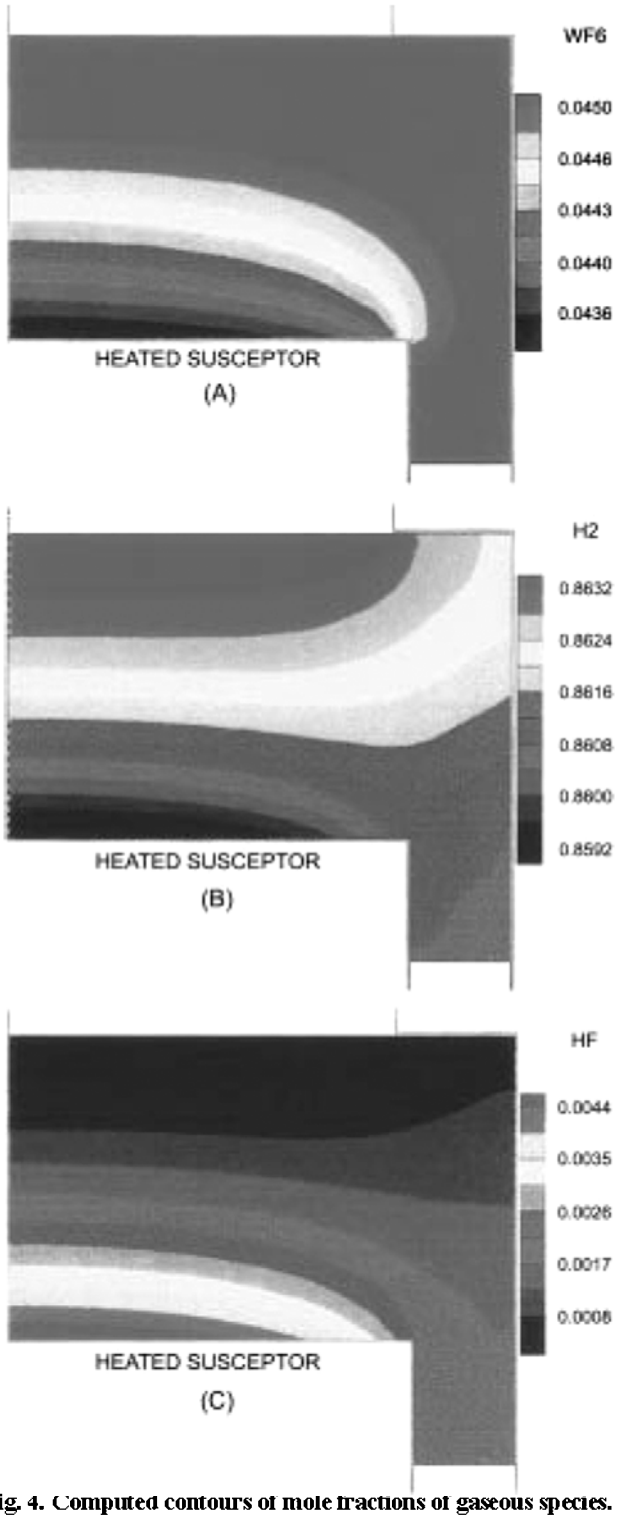

Fig. 4. Computed contours of mole fractions of gaseous species. (A) WF_6, (B) H_2, (C) HF

what near the hot wafer surface due to the large local temperature gradients. The Soret effect plays a minor role under the conditions of this simulation. Fig. 4c shows contours of hydrogen fluoride mole fraction. HF is produced by Eq. (1) on the reactive surfaces and diffuses back into the reactor zone.

Fig. 5 shows the total deposition rate as a function of wafer radius.

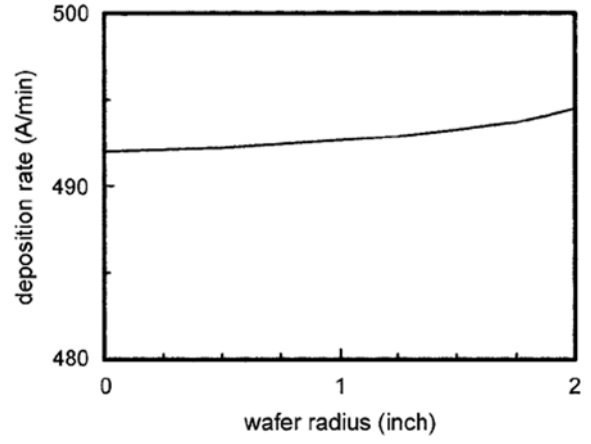

Fig. 5. Deposition rate distribution in a four-inch wafer.

The deposition rate at any point on the wafer is calculated by Eq. (16). Average deposition rate across a wafer is approximately 493 Å/min. The dependence of the reaction rate on the local concentration and temperature above the wafer surface implies that the film deposition rate is a strong function of flow field near the susceptor. The local deposition rate of tungsten film can be expressed in terms of the local surface reaction rate at the wafer surface, based on Eq. (2).

Highly uniform deposition on the four-inch wafer is obtained under operating conditions used in this study. This result is consistent with previous simulation results presented by Kleijn et al. [1991]. However, a slight increase in deposition rates with radial position is mostly due to the radial gradients in reactant partial pressures at

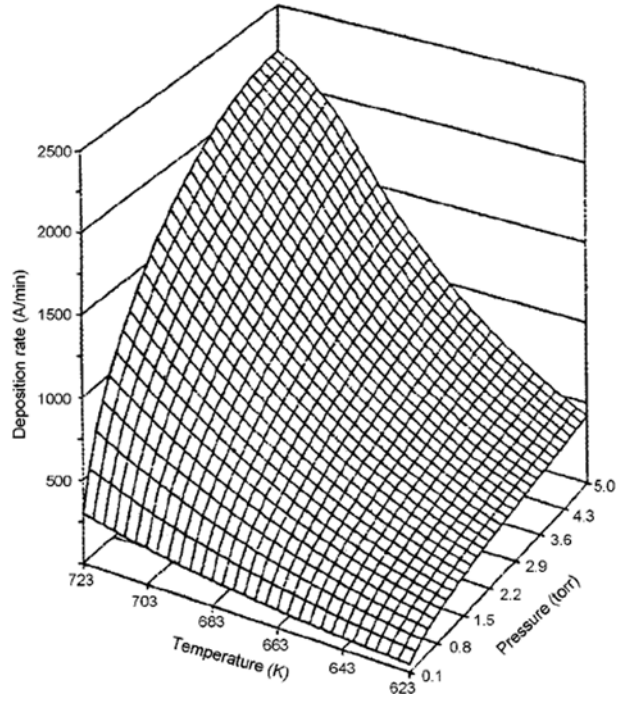

Fig. 6. Surface plot of deposition rate as functions of pressure and wafer temperature. Operating conditions are total flow rate of 1,200 sccm and the ratio of H_2 to WF_6 of 10.

the wafer surface.

Fig. 6 shows the surface plot of deposition rates as a function of temperature and pressure for an inlet H_2/WH_6 ratio of 10 and total flow rate of 1,200 sccm, in order to demonstrate the influence of these two independent variables and their interaction. Other parameter values were the same as those used in the previous calculations. As the temperature and pressure increase, the deposition rate increases markedly. Thus, either temperature or pressure or both may be adjusted to increase deposition rate. Since the deposition rate is exponentially dependent on temperature, as dictated in Eq. (2), a slight increase in temperature creates a large change in the deposition rate.

2. Comparison of Predicted and Experimental Results

The predicted deposition rates of tungsten LPCVD have been compared with some available experimental data published in the literature, e.g., Broadbent and Ramiller [1984], van der Putte [1987] and Kleijn et al. [1991]. For differential gradientless operating conditions or low conversion levels of reactants, it is meaningful to compare the model results with experimental ones even though the reactor configurations are not the same. The fractional utilization of WF_6 in tungsten LPCVD is quite low for the typical operating conditions in the experiments considered and the reactant compositions are fairly uniform throughout the reactor, as discussed by Arora and Pollard [1991]. Under these circumstances, comparison of available experimental data with model predictions is reasonable although the SWR used in this study is different from experimental reactor types, e.g. a horizontal reactor used by Broadbent and Ramiller and a pancake reactor by van der Putte.

Fig. 7 shows the model predictions and experimental results reported by Broadbent and Ramiller for the average deposition rates as functions of the wafer temperature. The model predictions agree well with the experimental data. The WF_6 partial pressure used in the experiments is relatively high (31.3 mtorr); therefore, the dependence of deposition rate on the WF_6 partial pressure is negligible. Fig. 8 shows the dependence of deposition rate on hydrogen inlet partial pressure. During these depositions, the WF_6 inlet partial pressure was held constant. Predicted deposition rates for various inlet hydrogen compositions agree well with experimental data reported

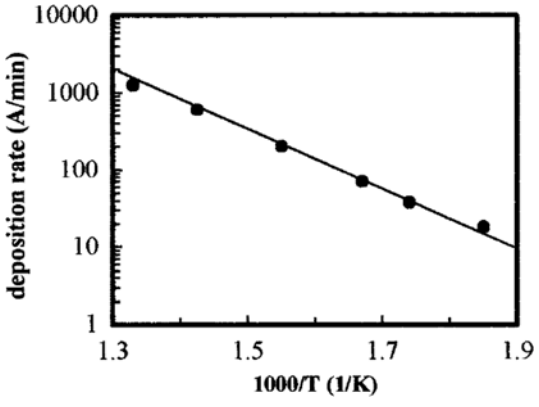

Fig. 7. Deposition rate versus inverse wafer temperature. Operating conditions are the pressure of 0.5 torr, the total flow rate of 1,700 sccm with H_2/WF_6 ratio of 15. Solid line is a model prediction and points are experimental data taken from Broadbent and Ramiller [1984].

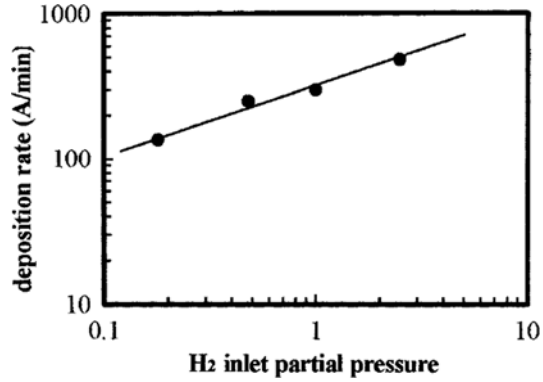

Fig. 8. Deposition rate as a function of hydrogen inlet partial pressure. Operating conditions are the wafer temperature of 643 K, the total flow rate of 1,700 sccm, and the partial pressure of WF_6 of 0.04 torr. Solid line is a model prediction and points are experimental data taken from Broadbent and Ramiller [1984].

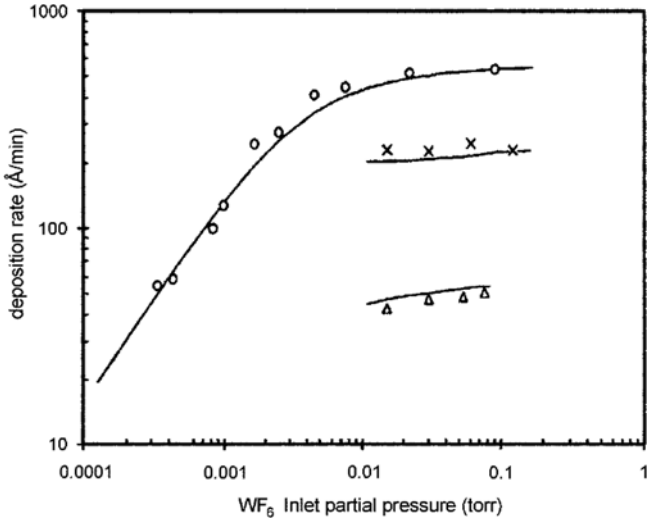

Fig. 9. Deposition rates as functions of WF_6 inlet partial pressure. Solid lines are model predictions and points are experimental data taken from literature: (○) Kleijn et al. [1991] for the wafer temperature of 673 K, the total flow rate of 1,200 sccm, and H_2 partial pressure of 0.833 torr; (×) Broadbent and Ramiller [1984] for the wafer temperature of 643 K, the total flow rate of 1,700 sccm, and H_2 partial pressure of 0.5 torr; (△) van der Putte [1987] for the wafer temperature of 573 K, the total flow rate of 1,200 sccm, and H_2 partial pressure of 0.75 torr.

by Broadbent and Ramiller. Fig. 9 shows the dependence of deposition rates on WF_6 partial pressure. The model closely predicts the experimental data for deposition rates as a function of WF_6 inlet pressure. This suggests that decreasing deposition rates at low WF_6 inlet pressures could be due to surface kinetics limitations rather than mass transfer limitations. A small lack of agreement between the model predictions and the data of Kleijn et al. is probably due to the reaction kinetic parameter values used. As a consequence, quite good agreement between the model predicted and experimental data is obtained for the tungsten deposition.

CONCLUSIONS

Process simulation is becoming an important tool for the development and optimization of CVD reactors and processes in order to minimize costly and time-consuming experiments. The main purpose of this study is to demonstrate how CVD mathematical modeling can be used to gain insight into LPCVD processes. The simulation is used to optimize operating conditions and reactor dimensions to provide good inter-wafer uniformity for tungsten deposition using the hydrogen reduction of tungsten hexafluoride. The same approach can be used to optimize operating conditions and reactor geometries for other deposition processes, e.g., atmospheric pressure CVD (APCVD) processes in multiple wafer reactors, assuming that validated reactor scale model is available. Although the simulation results are presented for a specific geometry and their validity is restricted to the range of operating parameters examined, the general approach used should be universally applicable.

A two-dimensional reactor model that incorporates fluid dynamics and transport phenomena in a single-wafer reactor is successfully applied to the tungsten CVD process over a range of operating conditions. The model solutions show that the gas flow forms smooth streamlines in the reactor. Simulations also indicate that large gradients in the temperature and concentrations across the wafer can be observed in cold wall single-wafer reactors.

For tungsten LPCVD from the hydrogen reduction of tungsten hexafluoride, the theoretical predictions of deposition rates, using a surface reaction rate expression which depends on the tungsten hexafluoride concentration, agree fairly well with experimental data. The good agreement between model predictions and experimental data demonstrates the validity of the modified rate expression used in this study.

ACKNOWLEDGMENT

The author appreciates the financial support of the Center for Industrial Technology at Inha Technical College.

APPENDIX

The density of the gas mixture is calculated by the equation of state using the species mass fraction and its molecular weight

$$\rho = \frac{P}{R_g T}\frac{\sum_{i=1}^{n}\omega_i}{\sum_{j=1}^{n}\omega_j/m_j}. \tag{A.1}$$

The viscosity of gaseous species in g/cm-sec is calculated by using the Chapman-Enskog theory [Reid et al., 1988]

$$\mu_i = 2.6693\times10^{-5}\frac{\sqrt{m_i T}}{\sigma_i^2\Omega_{\mu i}} \tag{A.2}$$

where σ_i is the collision diameter in Angstrom and the collision integral Ω_μ is defined by

$$\Omega_{\mu i} = \frac{1.1645}{T_i^{*0.14874}} + \frac{0.52487}{\exp(0.7732T_i^*)} + \frac{2.16178}{\exp(2.43787T_i^*)} \tag{A.3}$$

where $T_i^* = T(\kappa/\varepsilon)_i$. Values of σ and ε/κ for each species in this system are summarized in Table 1. Values for H_2 and HF are obtained from Svehla [1962], and value for WF_6 is estimated using $\tilde{V}_b$ =85.35 cm^3/mol and T_b=290 K [Park, 1992]. The viscosity of the gas mixture is computed from Wilke's formula, *viz.*

$$\mu_m = \sum_{j=1}^{n}\left(\frac{x_i\mu_i}{\sum_{j=1}^{n}x_j\Phi_{ij}}\right) \text{ with } \Phi_{ij} = \frac{1}{\sqrt{8}}\left(1+\frac{m_i}{m_j}\right)^{-1/2}\left[1+\left(\frac{\mu_i}{\mu_j}\right)^{1/2}\left(\frac{m_j}{m_i}\right)^{1/4}\right]^2 \tag{A.4}$$

Table 1. Intermolecular force constants and molecular weights

Species	σ (Å)	(ε/κ) (K)	m (g/mol)
Ar	3.542	93.3	39.94
H_2	2.827	59.7	2.02
HF	3.148	330.0	20.01
WF_6	5.134	342.0	297.86

Table 2. Coefficients for heat capacity in Eq. (A.5)

Species	α	β	γ
Ar	4.969	-7.670×10^{-6}	1.234×10^{-8}
H_2	6.874	9.263×10^{-5}	1.234×10^{-7}
HF	7.069	-5.401×10^{-4}	6.755×10^{-7}
WF_6	22.074	3.022×10^{-2}	-1.600×10^{-5}

The heat capacity for each species i is described by

$$c_{pi} = \alpha_i + \beta_i T + \gamma_i T^2. \tag{A.5}$$

Values for α, β and γ are given in Table 2, which are obtained by curve-fitting heat capacities in the literature [Chase et al., 1985; Pankratz, 1984]. The specific heat of the gas mixture is calculated by

$$c_{pm} = \sum_{i=1}^{n}\omega_i(c_{pi}/m_i). \tag{A.6}$$

The thermal conductivity of atomic gases is estimated by Eucken's correlation [Reid et al., 1988]

$$\lambda_i = \left(c_{pi} + \frac{5}{4}R_g\right)\frac{\mu_i}{m_i}. \tag{A.7}$$

The thermal conductivity of the gas mixture is computed by an expression analogous to Eq. (A.4)

The binary diffusion coefficients are calculated by using the Chapman-Enskog theory [Reid et al., 1988]

$$D_{ij} = 0.0018583\frac{\sqrt{T^3(1/m_i + 1/m_j)}}{P\sigma_{ij}^2\Omega_{D,ij}} \tag{A.8}$$

where $\sigma_{ij} = (\sigma_i + \sigma_j)/2$ and $(\varepsilon/\kappa)_{ij} = \sqrt{(\varepsilon/\kappa)_i(\varepsilon/\kappa)_j}$. The collision integral $\Omega_{D,ij}$ is analogous to that used in Eq. (A.3), *viz.*

$$\Omega_{D,ij} = \frac{1.06036}{T_{ij}^{*0.15610}} + \frac{0.19300}{\exp(0.47635T_{ij}^*)} + \frac{1.03587}{\exp(1.52995T_{ij}^*)} + \frac{1.76474}{\exp(3.89411T_{ij}^*)} \tag{A.9}$$

with $T_{ij}^* = T(\kappa/\varepsilon)_{ij}$. The diffusion coefficient of species i in a multi-

component mixture is calculated by Wilke's approximation

$$D_{im} = (1 - x_i)\left(\sum_{\substack{j=1 \\ j \neq i}}^{n} \frac{x_j}{D_{ij}}\right) \quad (A.10)$$

Multicomponent thermal diffusion coefficients are calculated by using the kinetic theory of gases based on the Lennard-Jones potential [Hirschfelder et al., 1954; Park, 1992].

NOMENCLATURE

c_p : molar heat capacity [cal/mole K or cal/g K]
D : diffusion coefficient [cm^2/sec]
D^T : thermal diffusion coefficient [g cm/sec]
G : deposition rate [Å/min]
g : gravitational acceleration [cm/sec^2]
m : molecular weight [g/mol]
n : number of gaseous species
p : pressure [torr or atm]
r : radial coordinate [cm]
R_g : universal gas constant [atm cm^3/mol K, or cal/mol K]
$\Re$: surface reaction rate [mol/cm^2 sec]
t : time [sec]
T : temperature [K]
T^* : reduced temperature [$\kappa T/\varepsilon$]
v : gas velocity [cm/sec]
x : mole fraction
z : axial coordinate [cm]

Greek Letters

ε : Lennard-Jones potential energy between two molecules [g cm^2/sec^2]
κ : Boltzmann's constant [$=3.30\times10^{-24}$ cal/K]
λ : thermal conductivity [cal/cm sec K]
μ : viscosity [g/cm sec]
ν : stoichiometric coefficient of the surface reaction
ρ : fluid density [g/cm^3]
σ : collision diameter for the Lennard-Jones parameter [Å]
ω : mass fraction

Superscripts and Subscripts

o : reactor inlet
i : index or species
j : index
m : mixture
r : radial direction
s : susceptor
T : thermal diffusion
w : wall
z : axial direction

REFERENCES

Arora, R. and Pollard, R., "A Mathematical Model for Chemical Vapor Deposition Influenced by Surface Reaction Kinetics: Application to low pressure deposition of tungsten," *J. Electrochem. Soc.*, **138**(5), 1523 (1991).

Blewer, R. S. (ed.), "Tungsten and Other Refractory Metals for VLSI Applications," MRS Publishers, Pittsburg, PA (1986).

Blewer, R. S. and McConica, C. M. (eds.), "Tungsten and Other Refractory Metals for VLSI Applications IV," MRS Publishers, Pittsburg, PA (1989).

Broadbent, E. K. (ed.), "Tungsten and Other Refractory Metals for VLSI Applications II," MRS Publishers, Pittsburg, PA (1987).

Broadbent, E. K. and Ramiller, C. L., "Selective Low Pressure Chemical Vapor Deposition of Tungsten," *J. Electrochem. Soc.*, **131**(6), 1427 (1984).

Bryant, W. A., "Kinetics of Tungsten Deposition by the Reaction of WF_6 and Hydrogen," *J. Electrochem. Soc.*, **125**(9), 1534 (1978).

Bullis, W. M. and O'Mara, W. C., "Large-Diameter Silicon Wafer Trends," *Solid State Technol.*, **36**(4), 59 (1993).

Cale, T. S., Jain, M. K. and Raupp, G. B., "Programmed Rate Processing to Increase Throughput in LPCVD," *J. Electrochem. Soc.*, **137**(5), 1526 (1990).

Cale, T. S., Park, J.-H., Raupp, G. B. and Jain, M. K., "Impacts of Temperature and Reactant Flow Rate Transients on LPCVD Tungsten Silicide Film Properties," in Rapid Thermal and Integrated Processing, Mat. Res. Soc. Symp. Proc., **224**, MRS, 171 (1991).

Cale, T. S., Park, J.-H., Gandy, T. H., Raupp, G. B. and Jain, M. K., "Step Coverage Predictions Using Combined Reactor Scale and Feature Scale Models for Blanket Tungsten LPCVD," *Chem. Eng. Comm.*, **119**, 197 (1993).

Cale, T. S., Raupp, G. B., Park, J. H., Jain, M. K. and Rogers, B. R., "The Inherently Transient Nature of Deposition Processes," in Proceedings of First International Conference of Transport Phenomena in Processing, Guceri, S., ed., Technomic Publishing Co., 127 (1992).

Campbell, S. A., Knutson, K. L., Ahn, K. H., Leighton, J. D. and Liu, B., "Gas Flow Patterns and Thermal Uniformity in Rapid Thermal Processing Equipment," *IEEE IEDM Technical Digest*, 921 (1990).

Chase, Jr. M. W., Davies, C. A., Downey, Jr. J. R., Frurip, D. J., McDonald, R. A. and Syverud, A. N., "JANAF Thermochemical Tables," *J. Phys. Chem. Ref. Data*, **14** (1985).

Chatterjee, S., Trachtenberg, I. and Edgar, T. F., "Mathematical Modeling of a Single-Wafer Rapid Reactor," *J. Electrochem. Soc.*, **139**(12), 3682 (1992).

Dobskin, D. M., "Kinetics and Uniformity of Deposition of Borophophosilicate Glass from Silane and Oxygen in a Single-Wafer Reactor," *J. Electrochem. Soc.*, **139**(9), 2573 (1992).

Economou, D. J. and Alkire, R. C., "A Mathematical Model for a Parallel Plate Plasma Etching Reactor," *J. Electrochem. Soc.*, **135**(11), 2786 (1988).

Finlayson, B. A., "Nonlinear Analysis in Chemical Engineering," McGraw-Hill Inc., New York (1980).

Fitzjohn, J. L. and Holstein, W. L., "Divergent Flow in Chemical Vapor Deposition Reactors," *J. Electrochem. Soc.*, **137**(2), 699 (1990).

Hasper, A., Holleman, J., Middelhoek, J. and Kleijn, C. R., "W-LPCVD Step Coverage and Modeling in Trenches and Contact Holes," in Tungsten and Other Advanced Metals for VLSI Applications, S. S. Wong and S. Furukawa, eds., MRS Publishers, Pittsburgh, PA, 127 (1990).

Hess, D. W., Jensen, K. F. and Anderson, T. J., "Chemical Vapor Deposition: A Chemical Engineering Perspective," *Rev. Chem. Eng.*, **3**(2), 97 (1985).

Hirschfelder, J. O., Curtiss, C. F. and Bird, R. B.: "Molecular Theory of Gases and Liquids," John Wiley & Sons, Inc. (1954).

Jasinski, T. J. and Kang, S. S., "Application of Numerical Modeling for CVD Simulation Test Case : Blanket Tungsten Deposition Uniformity," in Tungsten and Other Advanced Metals for ULSI Applications in 1990, G. C. Smith and R. Blumenthal, eds., MRS Publishers, Pittsburgh, PA, 219, (1991).

Jasinski, T. J. and Harshbarger, W. R., "Numerical Modeling of Tungsten Disilicide Deposition," in Tungsten and Other Refractory Metals for VLSI Applications IV, R. S. Blewer, C. M. McConica, ed., MRS Publishers, Pittsburgh, PA, 189 (1989).

Jenkinson, J. P. and Pollard, R., "Thermal diffusion Effects in Chemical Vapor Deposition Reactors," *J. Electrochem. Soc.*, **131**(12), 2911 (1984).

Jensen, K. F., "Micro-Reaction Engineering Applications of Reaction Engineering to Processing of Electronic and Photonic Materials," *Chem. Eng. Sci.*, **42**(5), 923 (1987).

Kleijn, C. R., Hoogendoorn, C. J., Hasper, A., Holleman, J. and Middelhock, J., "Transport Phenomena in Tungsten LPCVD in a Single-Wafer Reactor," *J. Electrochem. Soc.*, **138**(2), 509 (1991).

Kleijn, C. R., van der Meer, Th. H. and Hoogendoorn, C. J., "A Mathematical Model LPCVD in a Single Wafer Reactor," *J. Electrochem. Soc.*, **136**(11), 3423 (1989).

Kleijn, C. R., "A Mathematical Model of the Hydrodynamics and Gas-Phase Reactions in Silicon LPCVD in a Single-Wafer Reactor," *J. Electrochem. Soc.*, **138**(7), 2190 (1991).

Lam, D. K. and Koch, G. R., "Vacuum System Considerations for Plasma Etching Equipment," *Solid State Technol.*, **23**(9), 99 (1980).

McConica, C. M. and Krishnamani, K., "The Kinetics of LPCVD Tungsten Deposition in a Single Wafer Reactor," *J. Electrochem. Soc.*, **133**(12), 2542 (1986).

McConica, C. M. and Churchill, S., "Step Coverage Prediction During Blanket CVD Tungsten Deposition," in Tungsten and Other Refractory Metals for VLSI Applications III, V. A. Wells, ed., MRS Publishers, Pittsburgh, PA, 257 (1988).

Moslehi, M. M., Chapman, R. A., Wong, M., Paranjipe, A., Najm, H. N., Kuehne, J., Yekley, R. L. and Davis, C. j., "Single-Wafer Integrated Semiconductor Device Processing," *IEEE Trans. Electron Devices*, ED-**39**(1), 4 (1992).

Pankratz, L. B., "Thermodynamics Properties of Halides," U.S. Bureau of Mines, Bulletin 674 (1984).

Park, J.-H., "Deposition Uniformities on a Wafer and in a Trench for Tungsten Silicide LPCVD in a Single-Wafer Reactor," *Korean J. Chem. Eng.*, **13**, 105 (1996a).

Park, J.-H., "Programmed Rate Chemical Vapor Deposition to Decreasing Processing Time," *J. of Ind. & Eng. Chemistry*, **2**(2), 171 (1996b).

Park, J.-H., "Simulation of Low Pressure Chemical Vapor Deposition Using Combined Reactor Scale and Feature Scale Models," Ph.D Dissertation, Arizona State University, U.S.A. (1992).

Park, S.-K. and Economou, D. J., "Numerical Simulation of a Single-Wafer Isothermal Plasma Etching Reactor," *J. Electrochem. Soc.*, **137**(8), 2624 (1990).

Pauleau, Y. and Lami, Ph., "Kinetics and Mechanism of Selective Tungsten Deposition by LPCVD," *J. Electrochem. Soc.*, **132**(11), 2779 (1985).

Rana, V. V. S., Joshi, R. V. and Ohdomari, I., (eds.), "Advanced Metallization for ULSI Applications," MRS Publishers, Pittsburgh, PA (1992).

Reid, R. C., Prausnitz, J. M. and Poling, B. E., "The Properties of Gases & Liquids," McGraw-Hill, Inc., New York (1988).

Riely, P. E. and Clark, T. E., "Integrated Chemical Vapor Deposition and Plasma Etchback of Tungsten in Multichamber, Single-Wafer System," *J. Electrochem. Soc.*, **138**(10), 3008 (1991).

Rode, E. J. and Schmitz, J. E. J., "Study of Reactor Design by Computational Fluid Dynamics," in Advanced Metallization for ULSI Applications, V. V. S. Rana, R. V. Joshi, and I. Ohdomari, eds., MRS Publishers, Pittsburgh, 105 (1992).

Skelly, D. W., Lu, T.-M. and Woodruff, D. W., "Metallization Techniques," in VLSI Electronics: Microstructure Science, Academic Press, **15**, 101 (1987).

Smith, G. C. and Blumenthal, R. (eds.), "Tungsten and Other Advanced Metals for ULSI Applications in 1990," MRS Publishers, Pittsburgh, PA (1991).

Suwondo, E., Pibouleau, L., Domenech, S. and Riba, J. P., "Simulation via Orthogonal Collocation on Finite Element of a Chromatographic Column with Nonlinear Isotherm," *Chem. Eng. Comm.*, **102**, 161 (1991).

Svehla, R. A., "Estimated Viscosities and Thermal Conductivities of Gases at High Temperatures," NASA Tech. Report R-132, Lewis Res. Center, Cleveland, OH (1962).

Ulacia, F., Howell, J. I. S., Kmer, H. and Werner, Ch., "Flow and Reaction Simulation of a Tungsten CVD Reactor," *Appl. Sur. Sci.*, **38**, 370 (1989).

Van der Putte, P., "The Reaction Kinetics of the H_2 Reduction of WF_6 in the Chemical Vapor Deposition of Tungsten Films," *Philips J. Res.*, **42**, 608 (1987).

Werner, C., Ulacia, F. J. I., Hopfmann, C. and Flynn, P., "Equipment Simulation of Selective Tungsten Deposition," *J. Electrochem. Soc.*, **139**(2), 566 (1992).

Wong, F., "Single Wafer RTP-CVD Epitaxial Deposition Technology," *Solid State Technol.*, **32**(Oct.), 53 (1989).